Journal of Power Sources 275 (2015) 633–643

Contents lists available at ScienceDirect

Journal of Power Sources

journal homepage: www.elsevier.com/locate/jpowsour

Simplified electrochemical multi-particle model for $LiFePO_4$ cathodes in lithium-ion batteries

Mehrdad Mastali Majdabadi [a, *], Siamak Farhad [b], Mohammad Farkhondeh [c], Roydon A. Fraser [a], Michael Fowler [c]

[a] Mechanical and Mechatronic Engineering Department, University of Waterloo, 200 University Ave. West, Waterloo, ON N2L 3G, Canada
[b] Mechanical Engineering Department, University of Akron, Akron, OH 44325, United States
[c] Chemical Engineering Department, University of Waterloo, 200 University Avenue West, Waterloo, ON N2L 3G1, Canada

HIGHLIGHTS

- A model is developed to predict the performance of $LiFePO_4$ lithium-ion batteries.
- The developed model (SEMP model) is applicable to any composite cathode material.
- The SEMP model is applicable for charge/discharge rates as high as 5C.
- The computational time of this model is significantly reduced.
- A sensitivity analysis is done over battery design parameters using the SEMP model.

GRAPHICAL ABSTRACT

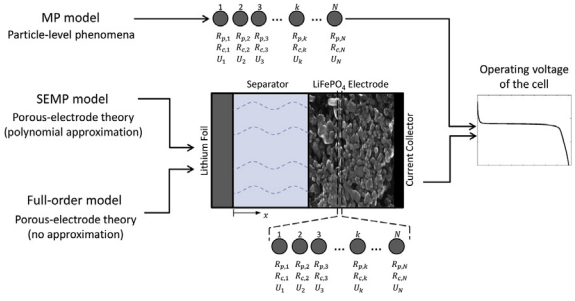

ARTICLE INFO

Article history:
Received 10 July 2014
Received in revised form
28 October 2014
Accepted 13 November 2014
Available online 14 November 2014

Keywords:
Lithium-ion battery
$LiFePO_4$
Reduced-order model
Simplified electrochemical multi-particle model

ABSTRACT

A simplified physics-based model is developed to predict the performance of an $LiFePO_4$ cathode at various operating and design conditions. Newman's full-order porous-electrode model is simplified using polynomial approximations for electrolyte variables at the electrode-level while a multi-particle model featuring variable solid-state diffusivity is employed at the particle level. The computational time of this reduced-order model is decreased by almost one order of magnitude compared to the full-order model without sacrificing the accuracy of the results. The model is general and can be used to expedite the simulation of any composite electrode with active-material particles of non-uniform properties (e.g., size, contact resistance, material chemistry etc.). In a broader perspective, this model is of practical value for electric vehicle power train simulations and battery management systems.

1. Introduction

Li-ion batteries are one of the best candidates as an energy storage system for automobile applications due to their high power and energy densities. Among various chemistries as their positive electrode (cathode), $LiFePO_4$ (LFP), first introduced by Padhi [1], has shown great performance and durability. Good thermal stability, low price, and low environmental impacts are other advantages of this cathode material [2]. However, poor electronic conductivity [3,4] and low apparent lithium diffusivity [5,6] are its main drawbacks, which are addressed by carbon coating and decreasing the

* Corresponding author.
E-mail address: mmastali@uwaterloo.ca (M. Mastali Majdabadi).

http://dx.doi.org/10.1016/j.jpowsour.2014.11.066
0378-7753/

particle size. The engineered $LiFePO_4$ is now commercialized and widely used in today's automotive-patterned Li-ion batteries necessitating the employment of reliable predictive models for design and control purposes.

The lithium insertion/deinsertion mechanism in LFP occurs through a two-phase process between Li-poor $Li_{\varepsilon}FePO_4$ and Li-rich $Li_{1-\varepsilon'}FePO_4$ phases (ε and $\varepsilon' << 1$). A proper model should ideally take this two-phase process into account while adequately capturing experimental charge/discharge data. However, the actual mechanism of LFP lithiation/delithiation dynamics has not accurately been decoded yet, thus no such an ideal model exist in the literature. A few mathematical models are proposed that simulate the complicated behavior of LFP each tackling a specific aspect of this material [7–18]. These models include the core–shell [7–9], phase field [10–12], resistive-reactant (RR) [13–15], and variable solid-state diffusivity (VSSD) [16–18] models. While the core–shell and phase-field models consider the two-phase process, the RR model does not consider any specific description for phase transformation. The VSSD model, on the other hand, is a simple yet physically descriptive model based on the concentration-dependent chemical diffusivity of the inserted lithium which mimics the coexistence of the two phases within particles. Although helpful in improving fundamental understanding of LFP lithiation/delithiation dynamics, these models have not been used for large-scale applications where fast and accurate computation is required.

Such large-scale applications of fast physics-based battery models include: i) battery management systems that require real-time estimation of the state-of-charge (SOC) and other battery states [19–22], and ii) thermal analysis of battery packs which involves simultaneous electrochemical-thermal simulation of a large number of inter-connected cells [23–26]. In both cases having accurate and computationally economic models that demand minimal computing resources is crucial. Therefore, simplified models which describe the characteristics of the smallest building block (i.e., cathode/separator/anode sandwich) of the battery during operation are being developed. The simplest model for the fast simulation of the cell performance is the single particle (SP) model wherein electrode-level losses (i.e., ionic and electronic transport across the cell) are ignored [27,28]. This assumption is reasonable for relatively low charge/discharge rates, thin, and highly conductive electrodes. If one of these conditions is violated, the model accuracy is noticeably degraded [28]. The SP model has been extended to a so-called "multi-particle (MP)" model to include an arbitrary number of particles. However, in the case of high rate/low temperature operating conditions where electrode-level losses are increased, implementation of porous-electrode theory becomes inevitable. Many mathematical methods have been proposed in the literature to speed up full-order porous-electrode models. These methods include but not limited to the perturbation techniques [29,30], residue grouping [31,32], proper orthogonal decomposition (POD) [33,34], and Galerkin's method [35]. The general strategy is to reduce the system of partial differential algebraic equations (PDAE) to a simpler model such as a system of differential algebraic equations (DAE) which are less computationally demanding. However, none of these methods have been used to simulate the electrochemical performance of cells containing electrodes with active-material particles of different sizes or non-uniform properties.

The objective of this paper is to develop an accurate yet computationally efficient model for Li-ion batteries that is able to handle an arbitrary number of active material particles. A simplified electrochemical multi-particle (SEMP) model is, therefore, developed and validated for the performance of a commercial LFP cathode. To this end, an MP model featuring VSSD formulation at the particle level is coupled with a simple polynomial approximation for the electrolyte variables at the electrode level making possible the prediction of the operating voltage of the cell at high charge/discharge rates.

2. Model development

The schematic of the half-cell modeled in this study is depicted in Fig. 1. The half-cell assembly is made of a $LiFePO_4$ porous-electrode, a Li foil counter/reference electrode, a porous separator, and the electrolyte that fills the pores of the electrode and separator. The LFP electrode contains N particles that may vary in radius, $R_{p,k}$, contact resistance, $R_{c,k}$, and/or potential U_k. Such a multi-particle description may be applied to any porous electrode with significant non-uniformity of active material properties among particles.

During discharge, the electrochemical reaction occurs at the surface of LFP particles leading to an inward flux of Li to the particles and during charge, the process proceeds in the reverse direction from the fully lithiated toward the fully delithiated form. This reaction is represented by Equation (1) as follows:

$$Li_y^+ + e^- + FePO_4 \underset{\text{charge}}{\overset{\text{discharge}}{\rightleftharpoons}} Li_yFePO_4 \qquad (1)$$

This section is started by describing the MP model and will be concluded with a modified porous-electrode model embedding multi-particle feature (SEMP model).

2.1. Multi-particle (MP) model

To assist with the implementation and realization, the MP model of [17] is described here providing additional explanations. In general, there exist non-uniform distributions of physical and/or chemical properties of active material (such as particle size, surface resistance, or equilibrium potential) in a porous electrode which

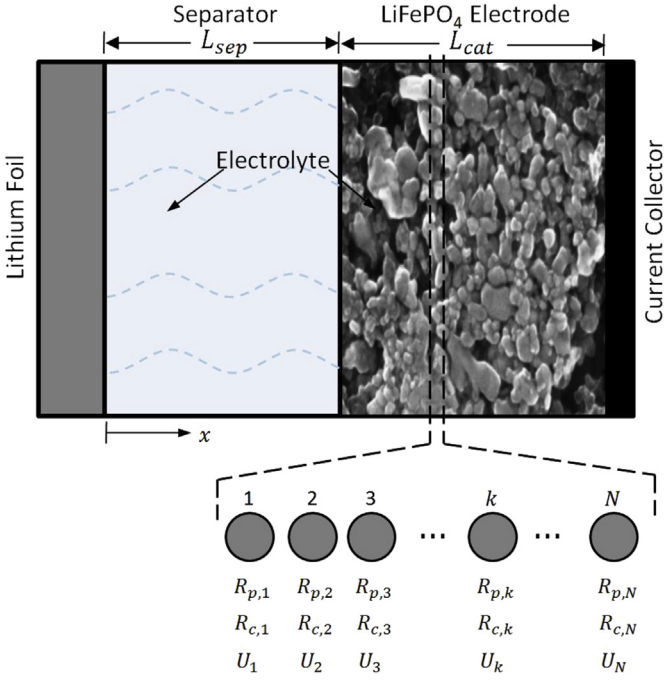

Fig. 1. Schematic of a half-cell containing Li foil, $LiFePO_4$ porous electrode, porous separator, and the electrolyte in the pores. The LFP cathode is assumed to contain multiple particle sizes that are assumed to be spherical.

may significantly affect its electrochemical performance. The MP model can be regarded as an extension of the SP model and emerges where more than one particle is required to give a proper account of the particle-level phenomena. Similar to the SP model [27,28], the MP model assumes that all of the electrode active material is exposed to the same electronic and ionic environment. In other words, the variations of the solid-phase and liquid-phase electric potentials as well as the species concentration in the electrolyte across the cell are neglected [27,28]. Instead, a simplistic representation of electrode-level losses is devised as an "equivalent Ohmic resistance" into which all of these limitations are lumped. The operating voltage of the cell will then be

$$V_{\text{cell}} = \Phi_{1,c} - \Phi_{1,f} - R_{\text{eq}} i_{\text{app}} \tag{2}$$

where, $\Phi_{1,c}$ is the cathode solid-phase potential, $\Phi_{1,f}$ is the Li foil potential, R_{eq} is the equivalent Ohmic resistance, and i_{app} is the applied current to the cell.

The VSSD concept is incorporated to account for Li transport losses inside each particle. This model, in fact, aggregates the bulk effects into a concentration-dependent diffusion coefficient and avoids explicit account of phase transformation and Li transport within the particles which have not been precisely depicted to date. The theory and complete derivation of the VSSD model can be found in Refs. [17,18]. This model gives the mass balance of Li inside the spherical particles as [17,18].

$$\frac{\partial c_{s,k}}{\partial t} = \frac{1}{r_k^2}\frac{\partial}{\partial r_k}\left(r_k^2 \alpha_k \mathscr{D} \frac{\partial c_{s,k}}{\partial r_k}\right) \tag{3}$$

where, the subscript k denotes the properties for the kth particle bin, $c_{s,k}$ is Li concentration inside the particles, r_k is the radial distance from the center of the particles, $\mathscr{D}$ is the solid-phase binary diffusion coefficient, and α_k is the thermodynamic factor defined as [17,18]:

$$\alpha_k = -\frac{F}{RT} y_k (1 - y_k) \frac{\partial U_k}{\partial y_k} \tag{4}$$

In Equation (4), F is the Faraday's constant, R is the universal gas constant, T is the temperature of the cell, $y_k = c_{s,k}/c_s^{\max}$ is the mole fraction of Li concentration inside the particles, and U_k is the equilibrium potential of the LFP particles. The boundary and initial conditions of Equation (3) are as follows [17,18]:

$$\frac{\partial c_{s,k}}{\partial r_k}(r_k = 0, t) = 0 \tag{5}$$

$$\alpha_k \mathscr{D} \frac{\partial c_{s,k}}{\partial r_k}\left(r_k = R_{p,k}, t\right) = \frac{i_{n,k}}{F} \tag{6}$$

$$c_{s,k}(r_k, t = 0) = c_{s,k}^0 \tag{7}$$

where, $R_{p,k}$ is the radius of particles, $c_{s,k}^0$ is the initial Li concentration inside the particles, and $i_{n,k}$ is the reaction current density at the surface of the k^{th} particle bin.

The reaction current density is calculated using Butler–Volmer equation:

$$i_{n,k} = i_k^0 \left[\exp\left(\frac{(1-\beta)F}{RT}\eta_k\right) - \exp\left(\frac{-\beta F}{RT}\eta_k\right)\right] \tag{8}$$

In Equation (8), β is the charge-transfer coefficient for LFP lithiation/delithiation and η_k is the surface overpotential of the LFP particle bins defined as $\eta_k = \Phi_{1,c} - R_{c,k} i_{n,k} - \Phi_2 - U_k$, where $R_{c,k}$ is the contact resistance between the LFP particles and conductive filler, and $\Phi_{1,c}$ and Φ_2 are the cathode and electrolyte potentials, respectively. In this study, the value of the contact resistance is set to zero and no resistive-reactant feature is included. Furthermore, i_k^0 is the exchange current density corresponding to the kth particle bin and is expressed as [18]:

$$i_k^0 = F k_c^0 c_s^{\max} c_e^{1-\beta} \tag{9}$$

where, k_c^0 is the reaction rate constant and c_e is the electrolyte concentration. The exchange current density is assumed to be independent of Li concentration at the surface of the LFP particles. This assumption is justified by noticing that during the discharge (charge), the surface concentrations rise (drop) to a large (small) values and remain almost constant during the whole process. Since the MP model does not include electrolyte losses, the Φ_2 and c_e are independent of time and space and their values are zero and c_e^0 (the initial electrolyte concentration), respectively.

The cell applied current is related to the reaction current densities at the surface of the particles through a charge balance as [17]:

$$\sum a_k i_{n,k} = -\frac{i_{\text{app}}}{L_{\text{cat}}} \tag{10}$$

where, L_{cat} is the thickness of the cathode and a_k is the specific surface area of the kth particle bin. The value of a_k is calculated by $3\varepsilon_k/R_{p,k}$ where ε_k is the volume fraction of the kth particle bin referred to the electrode volume. Equations (3)–(10) are then solved together to calculate the value of $\Phi_{1,c}$. Finally, the reaction overpotential at the Li foil is obtained using the Butler–Volmer equation as follows:

$$i_{\text{app}} = i_f^0 \left(\frac{c_e}{c_e^0}\right)^{1-\beta_f} \left[\exp\left(\frac{\beta_f F}{RT}\eta_f\right) - \exp\left(\frac{-\beta_f F}{RT}\eta_f\right)\right] \tag{11}$$

where, i_f^0 is the Li foil exchange current density based on a 1 M reference concentration, referred to the counter electrode area. β_f is the Li foil charge-transfer coefficient, and η_f is the overpotential of the Li foil defined as $\eta_f = \Phi_{1,f} - \Phi_2$. Having the values of $\Phi_{1,c}$ and $\Phi_{1,f}$ computed and the apparent Ohmic resistance of the cell, R_{eq}, fitted, the operating voltage of the Li/LFP half-cell is determined from Equation (2).

2.2. Simplified electrochemical multi-particle (SEMP) model

The described MP model is only valid for low to medium charge/discharge rates (i.e., up to 1C) where the overall electrode potential loss is primarily affected by the charge-transfer kinetics at the surface and diffusion through the bulk of active material particles. At higher rates, the potential loss originates not only from particle-level phenomena, but also from electrode-level electronic and ionic transport limitations. As a result, the gradients of the electrolyte concentration and potential as well as the potential gradient in the solid phase must be taken into account [26,36,37]. The MP model may be incorporated into Newman's porous-electrode theory [38,39] with the concentrated-solution theory describing the transport of species in the electrolyte [40] and the Ohm's law describing the percolation resistance across the solid phase. Such a full-order model becomes computationally expensive when two or more particle bins are involved. It is also the case when multidimensional simulation of the cell (e.g., thermal analysis), repetitive simulations (e.g., high-rate aging simulation), or real-time state estimation (e.g., battery management system) are required.

For such applications, the model must be capable of accurately accounting for electrolyte limitations (as compared to the simplistic equivalent resistance, R_{eq}) yet avoiding the heavy computation duty associated with solving the particle-level equations at every mesh point across the cell thickness. To this end, the solutions of the governing PDEs at the electrode level are approximated in the simplified electrochemical multi-particle model using a method originally formulated in Ref. [29]. In this method, the spatial distribution of potential and concentration in the electrolyte are approximated by polynomials in the space variable x, i.e., along the cell thickness, while the transient effects are captured by incorporating time-dependent polynomial coefficients. Different polynomial orders were examined and, as shown in Fig. 2, a cubic polynomial is chosen for the electrolyte potential and concentration distributions of the cathode. The electrolyte concentration distribution across the separator is approximated by a quadratic polynomial while the distribution of the electrolyte potential in the separator is obtained by analytically solving the charge balance equation. These orders of the polynomials make the method as simple as possible while keeping the accuracy in an acceptable range.

The following equations describe the electrolyte concentration distributions in the separator and cathode [36]:

$$c_{e,\mathrm{sep}}(x_{\mathrm{sep}},t) = a_1(t)x_{\mathrm{sep}}^2 + a_2(t)x_{\mathrm{sep}} + a_3(t), 0 \le x_{\mathrm{sep}} \le 1 \quad (12)$$

$$c_{e,\mathrm{cat}}(x_{\mathrm{cat}},t) = b_1(t)x_{\mathrm{cat}}^3 + b_2(t)x_{\mathrm{cat}}^2 + b_3(t)x_{\mathrm{cat}} + b_4(t), 0 \le x_{\mathrm{cat}} \le 1 \quad (13)$$

where, x_{sep} and x_{cat} are dimensionless length along the separator and cathode, respectively, and are defined as

$$x_{\mathrm{sep}} = \frac{x}{L_{\mathrm{sep}}}, 0 \le x \le L_{\mathrm{sep}} \quad (14)$$

$$x_{\mathrm{cat}} = \frac{(x - L_{\mathrm{sep}})}{L_{\mathrm{cat}}}, L_{\mathrm{sep}} \le x \le L_{\mathrm{sep}} + L_{\mathrm{cat}} \quad (15)$$

L_{sep} is the separator thickness and x is measured from the Li foil/separator interface across the cell. By incorporating the dimensionless lengths, the electrolyte mass balance equations [38,39] take the following form:

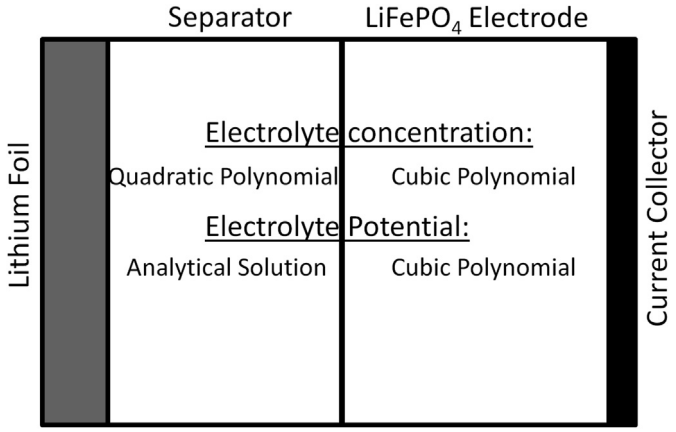

Fig. 2. The degree of approximated polynomials for the concentration and potential of the electrolyte in the separator and cathode.

$$\varepsilon_{\mathrm{sep}}\frac{\partial c_{e,\mathrm{sep}}}{\partial t} = \frac{1}{L_{\mathrm{sep}}^2}\frac{\partial}{\partial x_{\mathrm{sep}}}\left(D_{\mathrm{sep}}^{\mathrm{eff}}\frac{\partial c_{e,\mathrm{sep}}}{\partial x_{\mathrm{sep}}}\right) \quad (16)$$

$$\varepsilon_{\mathrm{cat}}\frac{\partial c_{e,\mathrm{cat}}}{\partial t} = \frac{1}{L_{\mathrm{cat}}^2}\frac{\partial}{\partial x_{\mathrm{cat}}}\left(D_{\mathrm{cat}}^{\mathrm{eff}}\frac{\partial c_{e,\mathrm{cat}}}{\partial x_{\mathrm{cat}}}\right) + \frac{(1-t_+^0)}{F}\sum a_k i_{n,k} \quad (17)$$

and the corresponding boundary conditions are:

$$\frac{\partial c_{e,\mathrm{sep}}}{\partial x_{\mathrm{sep}}}(x_{\mathrm{sep}} = 0, t) = -\frac{i_{\mathrm{app}}(1-t_+^0)L_{\mathrm{sep}}}{FD_{\mathrm{sep}}^{\mathrm{eff}}} \quad (18)$$

$$\frac{\partial c_{e,\mathrm{cat}}}{\partial x_{\mathrm{cat}}}(x_{\mathrm{cat}} = 1, t) = 0 \quad (19)$$

$$c_{e,\mathrm{sep}}(x_{\mathrm{sep}} = 1, t) = c_{e,\mathrm{cat}}(x_{\mathrm{cat}} = 0, t) \quad (20)$$

$$-\frac{D_{\mathrm{sep}}^{\mathrm{eff}}}{L_{\mathrm{sep}}}\frac{\partial c_{e,\mathrm{sep}}}{\partial x_{\mathrm{sep}}}(x_{\mathrm{sep}} = 1, t) = -\frac{D_{\mathrm{cat}}^{\mathrm{eff}}}{L_{\mathrm{cat}}}\frac{\partial c_{e,\mathrm{cat}}}{\partial x_{\mathrm{cat}}}(x_{\mathrm{cat}} = 0, t) \quad (21)$$

where, $\varepsilon_{\mathrm{sep}}$ is the separator porosity, $\varepsilon_{\mathrm{cat}}$ is the cathode porosity, and t_+^0 is the Li^+ ion transference number. $D_{\mathrm{cat}}^{\mathrm{eff}}$ and $D_{\mathrm{sep}}^{\mathrm{eff}}$ are the effective diffusion coefficients of the electrolyte in the cathode and separator, respectively. They are obtained according to $D_i^{\mathrm{eff}} = D_e\varepsilon_i^{\gamma}$ where the subscript i is cat or sep, D_e is the bulk electrolyte diffusivity, and γ is the Bruggeman exponent. Volume averaging of Equations (16) and (17) and using Equation (19) (i.e., the boundary condition at $x_{\mathrm{cat}} = 1$) yields:

$$\varepsilon_{\mathrm{sep}}\frac{\mathrm{d}c_{e,\mathrm{sep}}^{\mathrm{avg}}}{\mathrm{d}t} = \frac{1}{L_{\mathrm{sep}}^2}\left(D_{\mathrm{sep}}^{\mathrm{eff}}\frac{\partial c_{e,\mathrm{sep}}}{\partial x_{\mathrm{sep}}}(x_{\mathrm{sep}} = 1, t) - D_{\mathrm{sep}}^{\mathrm{eff}}\frac{\partial c_{e,\mathrm{sep}}}{\partial x_{\mathrm{sep}}}(x_{\mathrm{sep}} = 0, t)\right) \quad (22)$$

$$\varepsilon_{\mathrm{cat}}\frac{\mathrm{d}c_{e,\mathrm{cat}}^{\mathrm{avg}}}{\mathrm{d}t} = \frac{1}{L_{\mathrm{cat}}^2}\left(-D_{\mathrm{cat}}^{\mathrm{eff}}\frac{\partial c_{e,\mathrm{cat}}}{\partial x_{\mathrm{cat}}}(x_{\mathrm{cat}} = 0, t)\right) - \frac{(1-t_+^0)}{F}\frac{i_{\mathrm{app}}}{L_{\mathrm{cat}}} \quad (23)$$

The average concentrations are calculated by volume averaging Equations (12) and (13) over the separator and cathode, respectively, as:

$$c_{e,\mathrm{sep}}^{\mathrm{avg}}(t) = \frac{1}{3}a_1 + \frac{1}{2}a_2 + a_3 \quad (24)$$

$$c_{e,\mathrm{cat}}^{\mathrm{avg}}(t) = \frac{1}{4}b_1 + \frac{1}{3}b_2 + \frac{1}{2}b_3 + b_4 \quad (25)$$

In order to solve for the coefficients of concentration polynomials, seven independent equations are required. Substitution of the polynomial approximations (Equations (12) and (13)) and the average concentrations (Equations (24) and (25)) into Equations (18)–(23), gives the following set of six DAEs:

$$a_2 = -\frac{i_{\mathrm{app}}(1-t_+^0)L_{\mathrm{sep}}}{FD_{\mathrm{sep}}^{\mathrm{eff}}} \quad (26)$$

$$3b_1 + 2b_2 + b_3 = 0 \quad (27)$$

$$a_1 + a_2 + a_3 = b_4 \quad (28)$$

$$\frac{D_{sep}^{eff}}{L_{sep}}(2a_1+b_1)=\frac{D_{cat}^{eff}}{L_{cat}}b_3 \tag{29}$$

$$\frac{1}{3}\frac{da_1}{dt}+\frac{1}{2}\frac{da_2}{dt}+\frac{da_3}{dt}=\frac{2D_{sep}^{eff}}{\varepsilon_{sep}L_{sep}^2}a_1 \tag{30}$$

$$\frac{1}{4}\frac{db_1}{dt}+\frac{1}{3}\frac{db_2}{dt}+\frac{1}{2}\frac{db_3}{dt}+\frac{db_4}{dt}=-\frac{D_{cat}^{eff}}{\varepsilon_{cat}L_{cat}^2}b_3-\frac{1-t_+^0}{\varepsilon_{cat}F}\frac{i_{app}}{L_{cat}} \tag{31}$$

The last equations is obtained by solving the mass balance equation (Equation (17)) at one arbitrary point inside the cathode, $x_{cat,a}$, leading to [36]:

$$x_{cat,a}^3\frac{db_2}{dt}+x_{cat,a}^2\frac{db_2}{dt}+x_{cat,a}\frac{db_3}{dt}+\frac{db_4}{dt}=\frac{D_{cat}^{eff}}{\varepsilon_{cat}L_{cat}^2}(6b_1x_{cat,a}+2b_2)+\frac{(1-t_+^0)}{\varepsilon_{cat}F}\sum a_k i_{n,k}(x_{cat,a},t) \tag{32}$$

This equation requires the reaction current densities, $i_{n,k}$, to be calculated at $x_{cat,a}$ by solving particle-level equations (Equations (3)–(9)) at that location (i.e., plugging $\Phi_2(x_{cat,a},t)$ and $c_e(x_{cat,a},t)$ into Equations (8) and (9)).

Furthermore, it is assumed that the cell is at rest prior to discharge and the initial concentration of the electrolyte is uniform, c_e^0. This leads to zero value for all polynomial coefficients at $t=0$except for a_3 and b_4 whose initial values are equal to c_e^0. However, having zero initial value does not satisfy Equation (26) at $t=0$. To overcome this numerical issue, a dynamic behavior for the coefficient a_2 is artificially devised, that is, the value of a_2 is zero initially, but rapidly evolves to its value dictated by Equation (26). Such an arbitrary dynamics can be described as:

$$\frac{da_2}{dt}=-Aa_2-A\frac{i_{app}(1-t_+^0)L_{sep}}{FD_{sep}^{eff}} \tag{33}$$

where, A is a large number to guarantee rapid convergence of a_2 to its actual value. Solution of Equation (33) yields:

$$a_2=-\frac{i_{app}(1-t_+^0)L_{sep}}{FD_{sep}^{eff}}(1-\exp(-At)) \tag{34}$$

which replaces Equation (26) in the model. It should be noted that despite the absence of a rigorous local mass balance and, thus, unavoidable inaccuracies in approximating the electrolyte concentration and potential distributions, the polynomial profiles were chosen according to two criteria: i) minimum polynomial orders are considered in the model to minimize computational costs, and ii) the final operating voltage predictions of the model are accurate enough. In other words, similar to the non-conservative numerical algorithms such as finite-element and finite-difference methods, where the local mass balance is not rigorous (compared to the finite-volume method), the objective here is to obtain a sufficiently close approximation to the solution of the mass balance that meets the above criteria while maintaining computational efficiency. This approach resulted in a second order polynomial inside the separator and a third order polynomial inside the cathode as described in detail above. Therefore, the operating voltage of the cell is well captured with minimal computational cost.

After approximating the electrolyte concentration distribution, the potential distribution of the electrolyte is to be addressed. The charge balance inside the separator and the corresponding boundary conditions are formulated as [38,39]:

$$-\frac{\partial^2\Phi_{2,sep}}{\partial x_{sep}^2}+\frac{2RT(1-t_+^0)}{F}\frac{\partial}{\partial x_{sep}}\left(\frac{1}{c_{e,sep}}\frac{\partial c_{e,sep}}{\partial x_{sep}}\right)=0 \tag{35}$$

$$\Phi_{2,sep}(x_{sep}=0,t)=0 \tag{36}$$

$$-\frac{\kappa_{sep}^{eff}}{L_{sep}}\frac{\partial\Phi_{2,sep}}{\partial x_{sep}}(x_{sep}=1,t)=-\frac{\kappa_{cat}^{eff}}{L_{cat}}\frac{\partial\Phi_{2,cat}}{\partial x_{cat}}(x_{cat}=0,t) \tag{37}$$

κ_{sep}^{eff} is the effective electrolyte conductivity in the separator and is defined as $\kappa_{sep}^{eff}=\kappa\varepsilon_{sep}^{\gamma}$ where κ is the bulk ionic conductivity of the electrolyte, assumed to be constant. The electrolyte potential at the Li foil/separator interface is arbitrary set to zero as the reference electric potential of the electrolyte. Equations (35)–(37) are then solved analytically and the electrolyte potential distribution inside the separator is as follows:

$$\Phi_{2,sep}(x_{sep},t)=\frac{2RT(1-t_+^0)}{F}\ln\frac{a_1x_{sep}^2+a_2x_{sep}+a_3}{a_3}+\left(\frac{\kappa_{cat}^{eff}L_{sep}}{\kappa_{sep}^{eff}L_{cat}}c_3-\frac{2RT(1-t_+^0)}{F}\frac{2a_1+a_2}{a_1+a_2+a_3}\right)x_{sep} \tag{38}$$

where, c_3 is the third coefficient in the cubic polynomial approximation of the electrolyte potential across the cathode.

The cathode electrolyte potential is then approximated using the following cubic polynomial:

$$\Phi_{2,cat}(x_{cat},t)=c_1(t)x_{cat}^3+c_2(t)x_{cat}^2+c_3(t)x_{cat}+c_4(t) \tag{39}$$

The charge balance in the cathode and the corresponding boundary conditions are:

$$-\frac{\partial^2\Phi_{2,cat}}{\partial x_{cat}^2}+\frac{2RT(1-t_+^0)}{F}\frac{\partial}{\partial x_{cat}}\left(\frac{1}{c_{e,cat}}\frac{\partial c_{e,cat}}{\partial x_{cat}}\right)=\frac{L_{cat}^2}{\kappa_{cat}^{eff}}\sum a_k i_{n,k} \tag{40}$$

$$\frac{\partial\Phi_{2,cat}}{\partial x_{cat}}(x_{cat}=1,t)=0 \tag{41}$$

$$\Phi_{2,cat}(x_{cat}=0,t)=\Phi_{2,sep}(x_{sep}=1,t) \tag{42}$$

where, κ_{cat}^{eff} is the effective electrolyte conductivity in the cathode and is defined as $\kappa_{cat}^{eff}=\kappa\varepsilon_{cat}^{\gamma}$. By employing the boundary conditions for the electrolyte potential and concentration, volume-averaged charge balance equation reads:

$$\frac{\partial\Phi_{2,cat}}{\partial x_{cat}}(x_{cat}=0,t)-\frac{2RT(1-t_+^0)}{F}\left(\frac{1}{c_{e,cat}}\frac{\partial c_{e,cat}}{\partial x_{cat}}\right)\Big|_{x_{cat}=0}=-\frac{i_{app}L_{cat}}{\kappa_{cat}^{eff}} \tag{43}$$

The approximate solution for $\Phi_{2,cat}$ (Equation (39)) is then substituted into Equations (41)–(43) to give the following three equations for the polynomial coefficients of the electrolyte potential:

$$3c_1+2c_2+c_3=0 \tag{44}$$

$$c_4 = \frac{2RT(1-t_+^0)}{F}\ln\frac{a_1(t)+a_2(t)+a_3(t)}{a_3(t)} + \frac{\kappa_{cat}^{eff}L_{sep}}{\kappa_{sep}^{eff}L_{cat}}c_3 - \frac{2RT(1-t_+^0)}{F}\frac{2a_1+a_2}{a_1+a_2+a_3} \quad (45)$$

$$c_3 - \frac{2RT(1-t_+^0)}{F}\frac{b_3}{b_4} = -\frac{i_{app}L_{cat}}{\kappa_{cat}^{eff}} \quad (46)$$

The estimation of Equation (40) on the arbitrary point in the cathode, $x_{cat,a}$, gives the last required equation:

$$-(6c_1x_{cat,a}+2c_2) + \frac{2RT(1-t_+^0)}{F}\left(\frac{1}{c_{e,cat}}\frac{\partial c_{e,cat}}{\partial x_{cat}}\right)\Big|_{x_{cat}=0} = \frac{I_{cat}^2}{\kappa_{cat}^{eff}}\sum a_k i_{n,k}(x_{cat,a},t) \quad (47)$$

where, the second term on the left-hand-side is calculated using the estimated cathode concentration polynomial. The reaction current densities appeared on the right-hand-side of Equation (47) are obtained at $x_{cat,a}$ in the same way as described earlier for Equation (32).

In summary, one quadratic polynomial (Equation (12)) approximates the electrolyte concentration distribution in the separator while an analytic solution (Equation (38)) gives the potential distribution of the electrolyte in this region. Moreover, two cubic polynomials (Equations (13) and (39)) describe the concentration and potential distributions of the electrolyte across the cathode. The polynomial coefficients of Equations (12), (13) and (39) are calculated using Equations (26)–(32), (34), and (44)–(47). Finally, the estimated electric potential and concentration distributions of the electrolyte across the cathode are spatially averaged and fed back to the charge-transfer equations at the particle level (i.e., Φ_2 in Equation (8) and c_e in Equation (9)). Having incorporated these average values, the particle-level equations are solved simultaneously with the simplified electrode-level equations to give the electrode potential, $\Phi_{1,c}$.

In addition to the electrolyte simplifications, according to the recent multi-probe conductometric experiments, even though LFP is intrinsically insulating, applying carbon coating on its surface and addition of conductive filler significantly decrease the percolation resistivity of the composite electrode. As a result, it is not a limiting factor even at rates as high as 5C [18,41]. Hence, the electronic losses across the solid phase are ignored in this model (i.e., $\Phi_{1,c}$ is uniform across the electrode). The Cell voltage will eventually be the difference between the time-varying solid-phase potential $\Phi_{1,c}$ and the electric potential of the Li foil $\Phi_{1,f}$.

2.3. Solution procedure

In order to obtain operating voltage of the cell, the governing equations of the SEMP model are solved numerically using the finite element method in COMSOL Multiphysics software [42]. This model solves for the Li concentration inside the particles twice, one time to calculate the cathode potential based on the average values of the electrolyte potential and concentration and one time to estimate the polynomial coefficients based on the electrolyte variables at an arbitrary point inside the cathode, $x_{cat,a}$.The particles are discretized into 20 elements whose sizes gradually decrease while approaching the particle surfaces with the minimum to maximum element-size ratio of 0.2. As a result, the SEMP model requires solution of:

- $2 \times 20 \times N$ equations accounting for Li concentration inside the N particle bins,
- $2 \times N$ Butler–Volmer equations accounting for electrochemical reaction at the surface of the N particle bins,
- 1 equation for the Li foil potential, and,
- 11 equations to calculate the polynomial coefficients,

which form a system of $12 + 42 \times N$ partial differential algebraic equations that must be solved simultaneously. The full-order model, on the other hand, requires not only solving for Li concentration inside the particles but also for the dependent variables, $\Phi_{1,c}$, Φ_2, and c_e, across the thickness of the cell. If the cathode and separator are each discretized into 10 equal elements while the number of elements inside the particles remains the same as that in the SEMP model, the system of PDAEs for this model consists of $51 + 210 \times N$ equations, that is, $2 \times 2 \times 10$ equations for the electrolyte concentration and potential in the separator and cathode, 10 equations for the solid-phase potential in the cathode, 1 equation for the Li foil potential, $10 \times N$ equations for the electrochemical reactions at the surface of the N particle bins, and $10 \times 20 \times N$ equations for the Li concentration inside the N particle bins. The approximation becomes more computationally beneficial when a larger number of particle bins is required in the model.

3. Results and discussion

In this section, all the described models (full-order, SP, MP, and SEMP models) are separately implemented to predict a set of experimental galvanostatic discharge data obtained from the literature [18]. The experimental data consists of various operating rates from C/25 to 5C; thus, it can effectively examine the performance of the models over a wide operating range typical of that seen in electrified vehicles. The Newman's full-order model is used as an accurate benchmark to compare the SEMP model with whereas the SP an MP models are used to establish the limit of implementation simplicity and numerical facility. The required parameters are imported directly from Ref. [18] and are listed in Table 1 and Table 2. Four particle bins are considered to cover the wide PSD observed in SEM images. Among all, one particle bin (i.e., the 2nd bin) constitutes most of the active material volume fraction and is obtained from the actual PSD of the electrode (i.e., d_{50}). The rest of the particle sizes and volume fractions are fitted to capture

Table 1
List of parameters used in the models [18].

Parameter	Symbol	Value
Cathode charge-transfer coefficient	β	0.5
Li foil charge-transfer coefficient	β_f	0.5
Bruggeman exponent	γ	1.5
Initial salt concentration in the electrolyte (mol m^{-3})	c_e^0	1000
Maximum Li concentration in the LFP particles (mol m^{-3})	c_s^{max}	22,806
Solid-state binary diffusion coefficient (m^2 s^{-1})	$\mathscr{D}$	5×10^{-19}
Diffusion coefficient of the electrolyte (m^2 s^{-1})	D_e	5.2×10^{-10}
Porosity of the separator	ε_{sep}	0.6
Porosity of the cathode	ε_{cat}	0.5
Total active material volume fraction	ε_t	0.351
Reaction rate constant (mol m^{-2} s^{-1} (mol m^{-3})$^{-1.5}$)	k_c^0	2.5×10^{-13}
Li foil exchange current density (A m^{-2})	i_f^0	19
Separator thickness (m)	L_{sep}	675×10^{-6}
Cathode thickness (m)	L_{cat}	80×10^{-6}
Bulk ionic conductivity of electrolyte (S m^{-1})	κ	1.3
Effective electronic conductivity of the cathode (S m^{-1})	σ_{cat}^{eff}	6.75
Li$^+$ ion transference number	t_+^0	0.363
Temperature (K)	T	293.15
Geometric area of the electrode (m^2)	A_c	1.202×10^{-4}
Lower cut-off voltage (V)	V_{cut}^{min}	2.5
Upper cut-off voltage (V)	V_{cut}^{max}	4.1

the end capacities of the electrode. Details on the justification for, and empirical curve fitting approach to, determining the particle sizes and number of particles in the 4-particle PSD is beyond the scope of this article, but can be found in Refs. [17] and [18].

The electrode open-circuit potential (OCP) is approximated experimentally from low-rate galvanostatic discharge of the cell and is shown in Fig. 3a. Using this experimental pseudo OCP, the thermodynamic factor can then be calculated according to Equation (4) as shown in Fig. 3b.

The simulation results of the full-order model for the galvanostatic discharge rates from C/25 to 5C at 25 °C show good agreement with the experimental data and are presented in Fig. 4. These simulation results are used to assess the accuracy of the alternative models including the SP, MP, and SEMP models throughout this section. As the simplest approach, the SP model is used to simulate the full-range galvanostatic discharges and to see how the inclusion of an artificial Ohmic resistance at the electrode level improves the high-rate simulation results. The SP model is a special case of the MP model wherein only one particle bin is incorporated ($N = 1$). Therefore, the same equations used for the MP model (Equations (2)–(11)) are employed in the SP model with only one particle size. This particle size is chosen to be the d_{50} particle size (72 nm). The required model parameters are taken from Tables 1 and 2 as well as from Fig. 3a and b, and the value of R_{eq} is set to 2.15×10^{-3} Ohms (best fitted). As shown in Fig. 5, the SP model fails to predict the end-of-discharge capacities even at low discharge rates. Based on the transmission electron microscope (TEM) imaging of LFP electrodes, Srinivasan and Newman [7] attributed this effect to the inevitable presence of particle size distribution (PSD) in composite electrodes and unusually low apparent solid-phase diffusion coefficient of LFP. In addition, the error in the voltage predictions significantly enlarges as the applied current increases which is mainly caused by simplistically estimating the electrode-level losses using an equivalent Ohmic resistance, R_{eq} [36,37].

In order to predict the end-of-discharge capacities at different operating ranges, the particle size distribution should be considered in the model yielding the MP model [7]. In this model, the same particle bins as those in the full-order model (Table 2) are considered. Other parameters are set to be the same as the SP model. The simulation results are compared with the full-order model in Fig. 6. It is observed that, similar to the full-order model, the MP model can predict the end-of-discharge capacities at all discharge rates. This is due to the fact that both of these models ascribe the final capacities to the limitations of the sluggish diffusion (extremely low diffusion coefficient of 5×10^{-19} m^2 s^{-1}) inside the LFP particles for which the effect of size non-uniformities become significant. The attribution of end-capacities to the diffusion of host species within the insertion materials is intuitively acceptable for solid-solution materials and regularly yields successful results having only one particle bin incorporated. However, the need for introducing more than one LFP particle with different sizes to the model and the dependence of apparent (fitted) PSD on the applied current [18,43] disclose a more complicated

Table 2
The particle size distribution and their corresponding volume fraction used in the models [18].

Particle bin	Radius of particles (nm)	Volume fraction, $\varepsilon_k/\varepsilon_t$
1	22	0.36
2	36	0.42
3	62	0.12
4	169	0.10

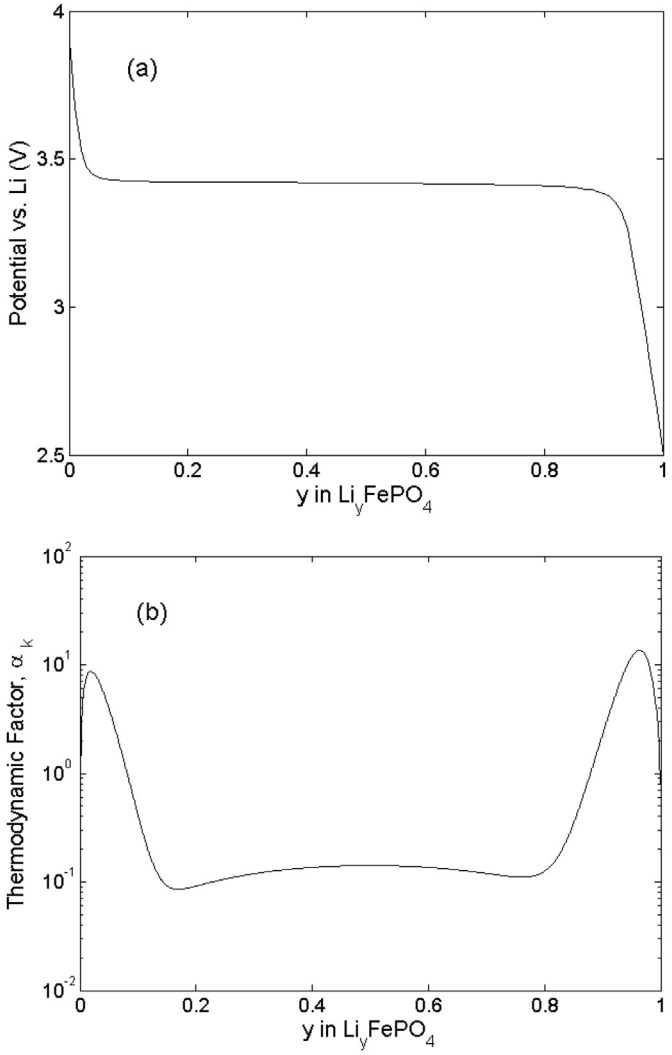

Fig. 3. (a) The equilibrium potential and (b) the thermodynamic factor, α_k, of the LFP cathode particles as a function of the Li mole fraction [18].

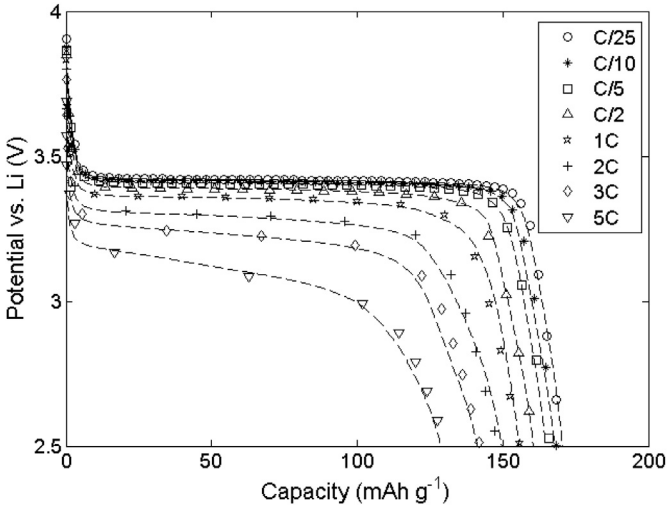

Fig. 4. Comparison between the experimental data (symbols) and simulation results of the Newman's full-order model (dashed lines) for the galvanostatic discharge rates from C/25 to 5C at 25 °C.

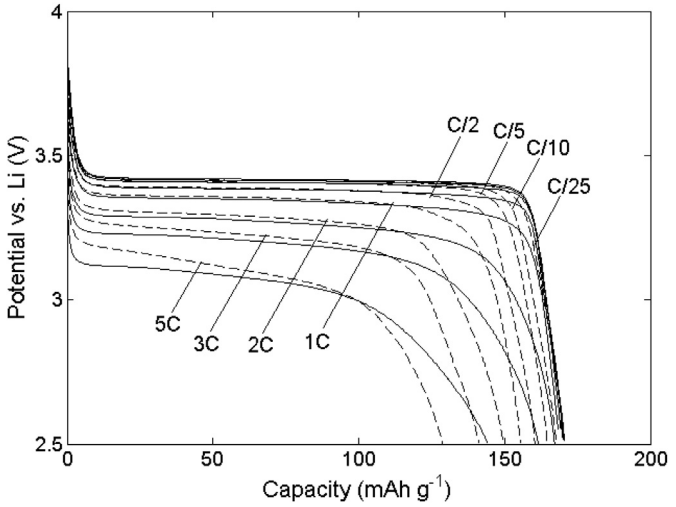

Fig. 5. Comparison between the Newman's full-order model (dashed lines) and simulation results of the SP model (solid lines) for the galvanostatic discharge rates from C/25 to 5C at 25 °C.

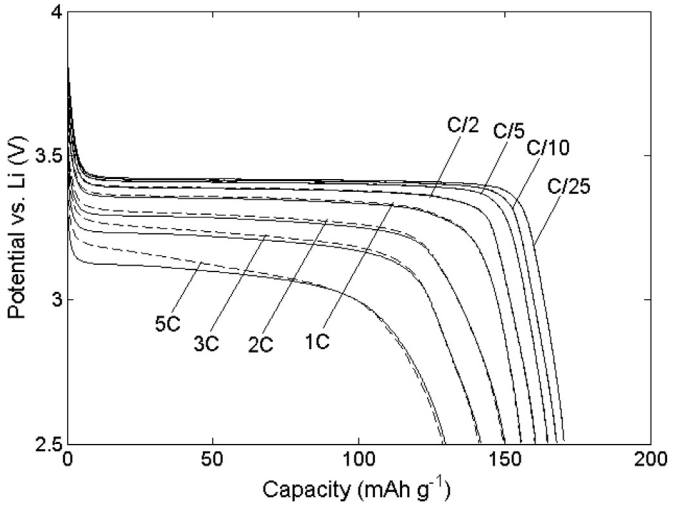

Fig. 6. Comparison between the Newman's full-order model (dashed lines) and simulation results of the MP model (solid lines) for the galvanostatic discharge rates from C/25 to 5C at 25 °C.

mechanism than a simple diffusion or a core–shell phase-change mechanism [44].

It is depicted in Fig. 6 that the MP simulation results successfully match the voltage–capacity curves obtained by the full-order model at the discharge rates up to the 1C. However, similar to the case of the SP model, the deviation between the two model predictions increases as the discharge rate increases. To maintain the simplicity and, at the same time, to improve the model accuracy, the MP model is extended to the SEMP model. Model parameters are taken to be the same as those used in the full-order model. In addition to these parameters, the location of the arbitrary point inside the LFP electrode, $x_{cat,a}$, introduces a new fitting parameter to the SEMP model. Since the mass and charge balance equations in the electrolyte must be satisfied at this point, its location can highly affect the obtained electrolyte concentration and potential distributions across the cell and hence the cell operating voltage. This parameter is estimated by manually fitting the voltage predictions of the SEMP model to the full-order model yielding the value of

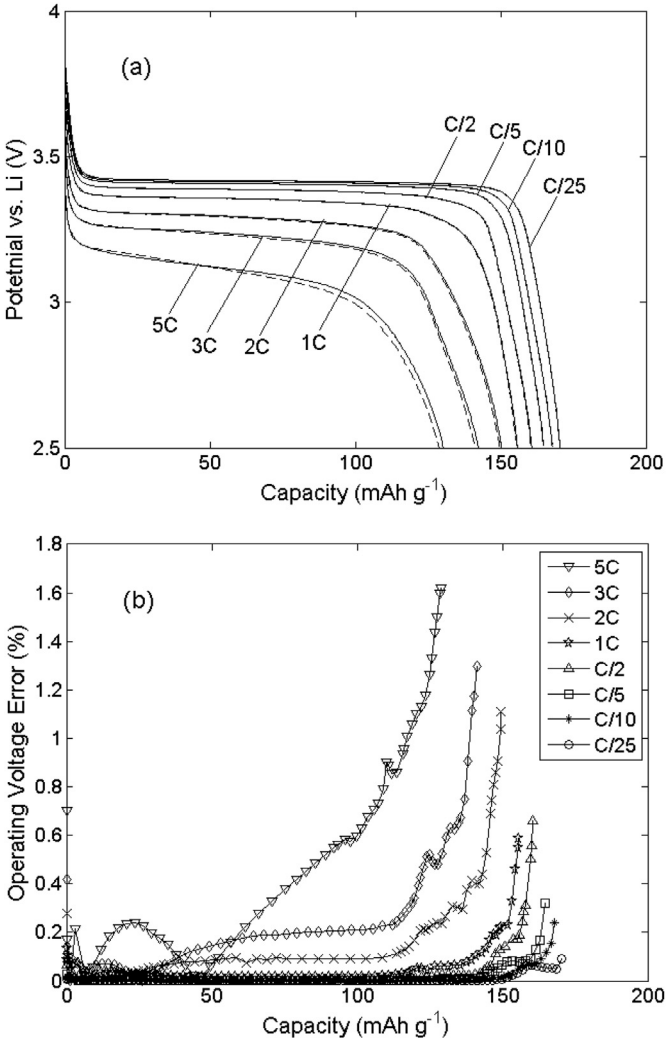

Fig. 7. (a) Comparison between the Newman's full-order model (dashed lines) and simulation results of the SEMP model (solid lines), and (b) the relative error of the SEMP model with respect to Newman's full-order model for the galvanostatic discharge rates from C/25 to 5C at 25 °C.

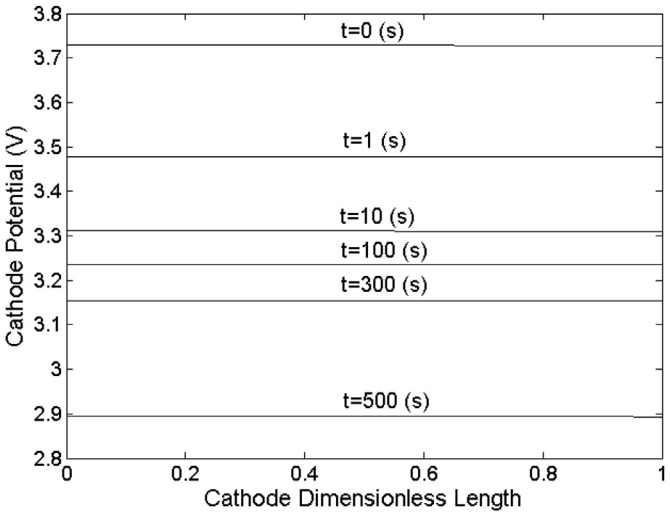

Fig. 8. Solid-phase potential distribution inside the cathode at various times and at 5C discharge rate obtained from the Newman's full-order model.

0.22 for $x_{cat,a}$ that is kept constant during all the simulations. In fact, there is some flexibility in the choice of this arbitrary location; it was varied to optimize the matching of results between the SEMP and those obtained using the Newman's full-order model.

The simulation results generated by the SEMP model is compared against those of the full-order model at the discharge rates from C/25 to 5C and are presented in Fig. 7a. The results show that the SEMP model can simulate not only the end-of-discharge capacities, but also the onset and slope of the voltage–capacity curves with high accuracy. The relative error of the model defined as $\text{abs}(V_{SEMP} - V_{full})/V_{full} \times 100$ is depicted in Fig. 7b where V_{SEMP} and V_{full} are the operating voltages of the cell predicted by SEMP and full-order models, respectively. It shows that even in the worst condition, which occurs at the end of 5C discharge, the relative error of the SEMP model does not exceed 1.7% highlighting the adequacy of the SEMP model relative to the full-order formulation.

The full-order model predictions of the solid-phase potential across the cathode are presented in Fig. 8. As it is observed, the solid-phase potential is almost constant across the electrode even at a rate as high as 5C, in line with our assumption in the SEMP model that the solid-phase potential depends only on time and not space. Very large discharge rates can, however, cause some solid-phase potential variations across the cathode, but they are not covered in this paper since the main focus here is on batteries for electric vehicles and plug-in vehicles applications for which a 5C discharge condition is aggressive. Some further analysis and descriptions on this subject may also be found in Appendix A.

In order to further investigate the accuracy of the SEMP model, a sensitivity analysis is attempted for design parameters such as the

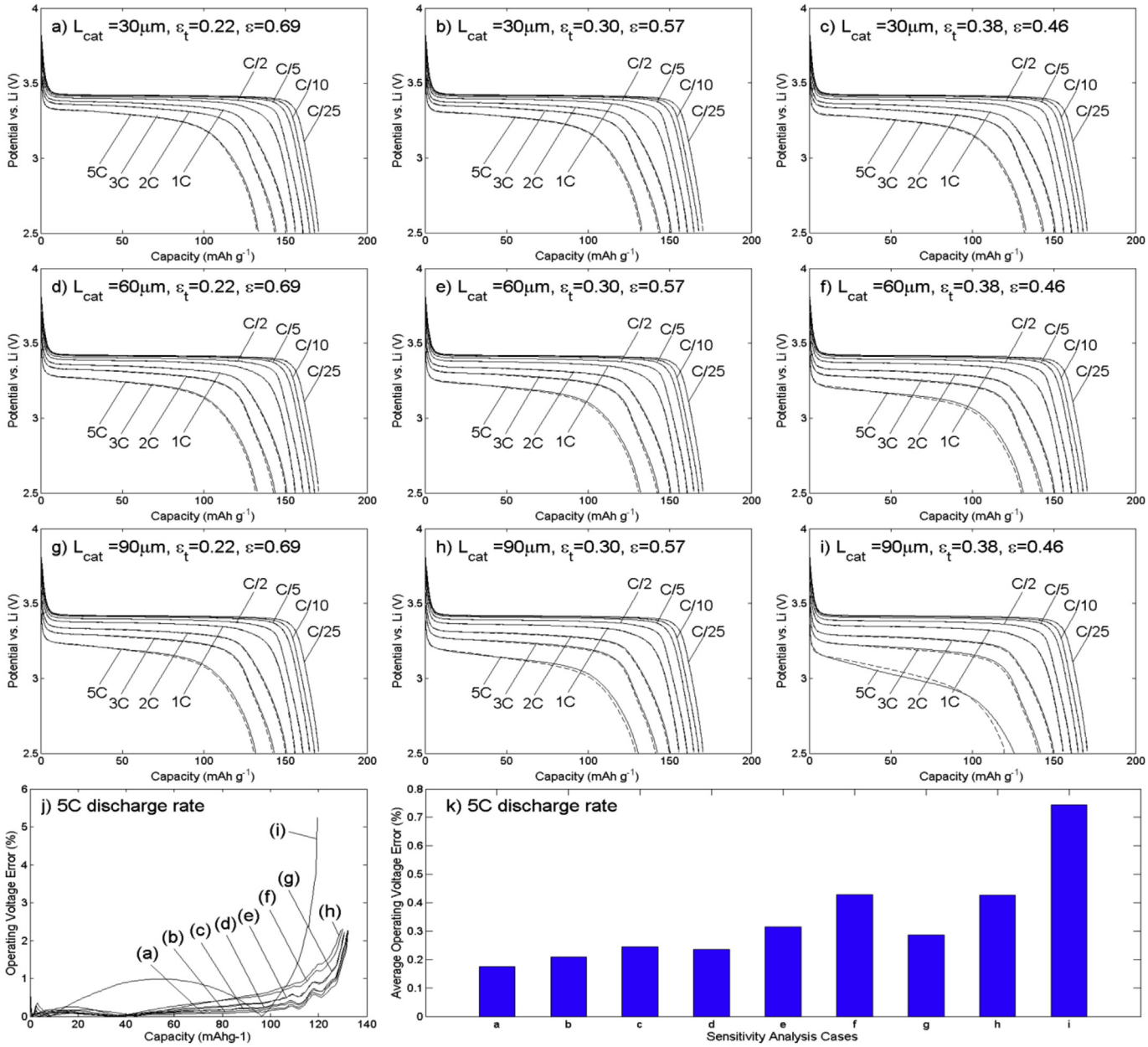

Fig. 9. (a–i) Comparison between the Newman's full-order (dashed lines) and SEMP models (solid lines) for discharge rates from C/25 to 5C at 25 °C in different cathode thicknesses (L_{cat}) from 30 nm to 90 μm, and cathode active material volume fractions (ε_t) from 0.22 to 0.38, (j) the relative, and (k) the average error of the SEMP model with respect to the Newman's full-order model at 5C discharge rates for different sensitivity analysis cases.

thickness and active material loading of the electrode. Three values for each parameter (30, 60, and 90 μm for the cathode thickness and 0.22, 0.3, 0.38 for the cathode active material volume fraction) are considered of which different combinations are examined while other model parameters are kept unchanged. It should be noted that enough attention has been paid to keep the ratio of the active material and conductive filler plus the binder constant when the active material volume fraction is changed; the higher active material loading, the higher binder/filler content and the lower porosity of the electrode. Fig. 9a–i shows the results of the full-order and SEMP models in all cases. In addition, the relative and average errors of the SEMP model at 5C discharge rate for all cases are depicted in Fig. 9j and k, respectively. The relative error is calculated from the same relation as used for Fig. 7b while the average error is defined as $\sum \mathrm{abs}(V_{\mathrm{SEMP}} - V_{\mathrm{full}})/\sum V_{\mathrm{full}} \times 100$ that is the area between the operating voltage curves predicted by the SEMP and full-order models divided by the area under the operating voltage curve of the full-order model. Fig. 9j shows that the maximum relative error of the SEMP model is about 2% in all cases except the case *i* where the electrolyte is almost depleted at the end of discharge and the error reaches to a maximum of 5%. Fig. 9k, however, demonstrates that in average incorporating the SEMP model yields the prediction error of less than 1%. As a result, good agreement between the results of the SEMP and the full-order models in all cases is observed and the developed SEMP model proved valid for a wide range of electrode designs.

4. Conclusion

In order to increase the computational efficiency in mathematical modeling of Li-ion batteries, a simple yet accurate multi-particle model was developed and validated for a known commercial LFP electrode. In this model, the Li insertion/deinsertion process into/out of LFP was modeled using the VSSD concept and four particle bins were considered to represent the apparent PSD of the cathode. In general, depending on the active materials used in the electrode and regardless of microscopic details of Li transport within the particles, including more than one particle bin with different intrinsic or geometric properties remains a common practice. To add the effects of the electrolyte, a polynomial approximation method was incorporated wherein the electrolyte variables are expressed as cubic and quadratic polynomials or solved analytically. The developed model was then compared with the full-order model. It was shown that although the number of involved equations is reduced by a factor of five, the predicted electrode potential matches well with the full-order simulation results for a wide range of operating conditions (with relative error less than 1.7%). The model was also successfully examined for various electrode designs proving it as a reliable and fast routine in place of full-order models for practical applications such as stack modeling of full-sized commercial batteries, aging studies, or in battery management systems.

Appendix A. The solid-phase potential across the electrode

In order to show the validity of ignoring the solid-phase potential gradient across the cathode, a simple calculation is present here. By considering constant reaction current density across the cathode, the Ohm's law is written as follows:

$$\frac{\partial}{\partial x_{\mathrm{cat}}}\left(\sigma_{\mathrm{cat}}^{\mathrm{eff}}\frac{\partial \Phi_{1,\mathrm{cat}}}{\partial x_{\mathrm{cat}}}\right) = L_{\mathrm{cat}} i_{\mathrm{app}} \tag{A.1}$$

and the corresponding boundary conditions are:

$$\left.\frac{\partial \Phi_{1,\mathrm{cat}}}{\partial x_{\mathrm{cat}}}\right|_{x_{\mathrm{cat}}=0} = 0 \tag{A.2}$$

$$\left.\frac{\partial \Phi_{1,\mathrm{cat}}}{\partial x_{\mathrm{cat}}}\right|_{x_{\mathrm{cat}}=1} = \frac{L_{\mathrm{cat}} i_{\mathrm{app}}}{\sigma_{\mathrm{cat}}^{\mathrm{eff}}} \tag{A.3}$$

This assumption enables us to perform a simple dimensional analysis without getting involved with complicated mathematical formulation. Solution of Equation (A.1) using its boundary conditions results in:

$$\Phi_{1,\mathrm{cat}} = \frac{L_{\mathrm{cat}} i_{\mathrm{app}}}{2\sigma_{\mathrm{cat}}^{\mathrm{eff}}} x_{\mathrm{cat}}^2 + C \tag{A.4}$$

where C is the an arbitrary unknown whose value can be obtained using the averaged potential of the cathode.

$$C = \Phi_{1,\mathrm{cat}}^{\mathrm{avg}} - \frac{L_{\mathrm{cat}} i_{\mathrm{app}}}{6\sigma_{\mathrm{cat}}^{\mathrm{eff}}} \tag{A.5}$$

By replacing C in the relation for $\Phi_{1,\mathrm{cat}}$, the final form of the cathode potential distribution is:

$$\Phi_{1,\mathrm{cat}} = \frac{L_{\mathrm{cat}} i_{\mathrm{app}}}{\sigma_{\mathrm{cat}}^{\mathrm{eff}}}\left(\frac{x_{\mathrm{cat}}^2}{2} - \frac{1}{6}\right) + \Phi_{1,\mathrm{cat}}^{\mathrm{avg}} \tag{A.6}$$

By noting the final form of the solid-phase potential distribution on the cathode and incorporating the parameter values from Table 1 ($L_{\mathrm{cat}} = 80 \times 10^{-6}$ m and $\sigma_{\mathrm{cat}}^{\mathrm{eff}} = 6.75\ \mathrm{Sm}^{-1}$), it is seen that the first two terms are of an order of $\mathrm{O}(10^{-5} i_{\mathrm{app}})$. On the other hand, the third term, average solid-phase potential, is of an order of $\mathrm{O}(1)$. As a result, to alter the solid-phase potential across the cathode, i_{app} has to take very large values. Therefore, the assumption of constant solid-phase potential across the cathode seems to be verified for the objective application of the electric vehicles.

References

[1] A.K. Padhi, K.S. Nanjundaswamy, J.B. Goodenough, J. Electrochem. Soc. 144 (1997) 1188.
[2] S.-Y. Chung, J.T. Bloking, Y.-M. Chiang, Nat. Mater. 1 (2002) 123.
[3] N. Ravet, J.B. Goodenough, S. Besner, M. Simoneau, P. Hovington, M. Armand, 196th Meet. Electrochem. Soc. (1999), 99-2, Abstr. # 127, Hawai.
[4] N. Ravet, Y. Chouinard, J.F. Magnan, S. Besner, M. Gauthier, M. Armand, J. Power Sources 97–98 (2001) 503.
[5] A. Yamada, S.C. Chung, K. Hinokuma, J. Electrochem. Soc. 148 (2001) A224.
[6] C. Delacourt, P. Poizot, S. Levasseur, C. Masquelier, Electrochem. Solid State Lett. 9 (2006) A352.
[7] V. Srinivasan, J. Newman, J. Electrochem. Soc. 151 (2004) A1517.
[8] U.S. Kasavajjula, C. Wang, P.E. Arce, J. Electrochem. Soc. 155 (2008) A866.
[9] S. Dargaville, T.W. Farrell, J. Electrochem. Soc. 157 (2010) A830.
[10] G.K. Singh, G. Ceder, M.Z. Bazant, Electrochim. Acta 53 (2008) 7599.
[11] D. Burch, G. Singh, G. Ceder, M.Z. Bazant, Solid State Phenom. 139 (2008) 95.
[12] D. Burch, M.Z. Bazant, Nano Lett. 9 (2009) 3795.
[13] K.E. Thomas-Alyea, ECS Trans. 16 (2008) 155.
[14] M. Safari, C. Delacourt, J. Electrochem. Soc. 158 (2011) A63.
[15] M. Safari, C. Delacourt, J. Electrochem. Soc. 158 (2011) A562.
[16] I.V. Thorat, Understanding Performance-limiting Mechanisms in Li-ion Batteries for High-rate Applications, Brigham Young University, 2009.
[17] M. Farkhondeh, C. Delacourt, J. Electrochem. Soc. 159 (2012) A177.
[18] M. Farkhondeh, M. Safari, M. Pritzker, M. Fowler, T. Han, J. Wang, C. Delacourt, J. Electrochem. Soc. 161 (2014) A201.
[19] G.L. Plett, J. Power Sources 134 (2004) 262.
[20] M. Mastali, J. Vazquez-Arenas, R. Fraser, M. Fowler, S. Afshar, M. Stevens, J. Power Sources 239 (2013) 294.
[21] R. Klein, N.A. Chaturvedi, J. Christensen, J. Ahmed, R. Findeisen, A. Kojic, IEEE Trans. Control Syst. Technol. 21 (2013) 289.
[22] S.J. Moura, N.A. Chaturvedi, M. Krstić, J. Dyn. Syst. Meas. Control 136 (2013) 011015.
[23] G.-H. Kim, K. Smith, K.-J. Lee, S. Santhanagopalan, A. Pesaran, J. Electrochem. Soc. 158 (2011) A955.
[24] H. Sun, X. Wang, B. Tossan, R. Dixon, J. Power Sources 206 (2012) 349.
[25] M. Guo, R.E. White, J. Power Sources 221 (2013) 334.

[26] N. Baba, H. Yoshida, M. Nagaoka, C. Okuda, S. Kawauchi, J. Power Sources 252 (2014) 214.
[27] S. Atlung, K. West, T. Jacobsen, J. Electrochem. Soc. 126 (1979) 1311.
[28] S. Santhanagopalan, Q. Guo, P. Ramadass, R.E. White, J. Power Sources 156 (2006) 620.
[29] V.R. Subramanian, V. Boovaragavan, V.D. Diwakar, Electrochem. Solid State Lett. 10 (2007) A255.
[30] V.R. Subramanian, V. Boovaragavan, V. Ramadesigan, M. Arabandi, J. Electrochem. Soc. 156 (2009) A260.
[31] K.A. Smith, C.D. Rahn, C.-Y. Wang, in: 2008 IEEE Int. Conf. Control Appl, IEEE, 2008, pp. 714–719.
[32] K.A. Smith, C.D. Rahn, C.-Y. Wang, J. Dyn. Syst. Meas. Control 130 (2008) 011012.
[33] L. Cai, R.E. White, J. Electrochem. Soc. 156 (2009) A154.
[34] L. Cai, R.E. White, J. Electrochem. Soc. 157 (2010) A1188.
[35] T.-S. Dao, C.P. Vyasarayani, J. McPhee, J. Power Sources 198 (2012) 329.
[36] S. Khaleghi Rahimian, S. Rayman, R.E. White, J. Power Sources 224 (2013) 180.
[37] W. Luo, C. Lyu, L. Wang, L. Zhang, J. Power Sources 241 (2013) 295.
[38] M. Doyle, T.F. Fuller, J. Newman, J. Electrochem. Soc. 140 (1993) 1526.
[39] K. Thomas, J. Newman, R. Darlin, Adv. Lithium-ion Batter, Kluwer Academic/Plenum Publishers, New York, 2002, pp. 345–392.
[40] J. Newman, K.E. Thomas-Alyea, Electrochemical Systems, third ed., Wiley Interscience, 2004.
[41] M. Ender, A. Weber, E. Ivers-Tiffée, Electrochem. Commun. 34 (2013) 130.
[42] COMSOL Multiphysics, User's Guide, Version 4.3b, COMSOL Inc., 2014.
[43] C. Delacourt, M. Safari, Electrochim. Acta 56 (2011) 5222.
[44] M. Safari, M. Farkhondeh, M. Pritzker, M. Fowler, T. Han, S. Chen, Electrochim. Acta 115 (2014) 352.

Nomenclature

a_k: specific surface area of the kth LFP particle bin, m^{-1}
c_e: electrolyte concentration, mol m^{-3}
c_e^0: initial electrolyte concentration, mol m^{-3}
$c_{s,k}$: Li concentration inside the kth LFP particle bin, mol m^{-3}
$c_{s,k}^0$: initial Li concentration inside the kth LFP particle bin, mol m^{-3}
c_s^{max}: maximum Li concentration in the LFP particles, mol m^{-3}
$\mathscr{D}$: solid-state binary diffusion coefficient, $m^2\ s^{-1}$
D_e: electrolyte diffusion coefficient, $m^2\ s^{-1}$
F: Faraday's constant, 96,487 C mol^{-1}
i_{app}: total current density of the cell, A m^{-2}
i_k^0: exchange current density of the kth LFP particle bin, A m^{-2}
i_f^0: exchange current density of Li foil counter electrode based on a 1 M reference concentration, referred to the counter electrode area, A m^{-2}
$i_{n,k}$: reaction current density at the surface of the kth LFP particle bin, A m^{-2}
k_c^0: electrochemical reaction constant of the LFP electrode, mol $m^{-2}\ s^{-1}$ $(mol\ m^{-3})^{-1.5}$
L: component thickness, m
r: radial distance from the center of the particles, m
R: universal gas constant, 8.314 J $mol^{-1}\ K^{-1}$
$R_{c,k}$: conductive-matrix/active material interparticle resistance for the kth LFP particle bin, $\Omega\ m^2$
R_{eq}: equivalent Ohmic resistance of the cell, $\Omega\ m^2$
$R_{p,k}$: radius of the kth LFP particle, m
t: time, s
T: temperature, K
t_+^0: Li^+ transference number
U_k: OCP of the kth LFP particle bin vs. Li, V
V_{cell}: operating voltage of the cell, V
x: distance from the Li foil/separator interface inside the cell, m
$x_{cat,a}$: arbitrary point inside the cathode, m
y_k: mole fraction of the Li concentration in the kth LFP particle bin
α_k: thermodynamic factor of the kth LFP particle bin
β: charge-transfer coefficient of the LFP electrode
β_f: charge-transfer coefficient of Li foil
ε: component porosity
ε_k: volume fraction of the kth LFP particle bin per unit volume of the electrode
ε_t: total volume of the cathode active material per unit volume of the electrode
η_k: surface overpotential of the kth LFP particle bin, V
η_f: surface overpotential of Li foil, V
γ: Bruggeman exponent, 1.5
κ: ionic conductivity of the electrolyte, S m^{-1}
$\Phi_{1,c}$: electrical potential of the cathode, V
$\Phi_{1,f}$: electrical potential of Li foil, V
Φ_2: electrical potential of the electrolyte, V
σ: bulk electronic conductivity of the cathode, S m^{-1}

Subscript

cat: cathode
sep: separator

Superscript

avg: averaged value
eff: effective value